Biosensors and Bioelectronics 176 (2021) 112921

Contents lists available at ScienceDirect

Biosensors and Bioelectronics

journal homepage: http://www.elsevier.com/locate/bios

An ultrasensitive impedance biosensor for *Salmonella* detection based on rotating high gradient magnetic separation and cascade reaction signal amplification

Fengchun Huang [a], Li Xue [a], Wuzhen Qi [a], Gaozhe Cai [a], Yuanjie Liu [b], Jianhan Lin [b,*]

[a] Key Laboratory of Agricultural Information Acquisition Technology, Ministry of Agriculture and Rural Affairs, China Agricultural University, Beijing, China
[b] Key Laboratory of Modern Precision Agriculture System Integration Research, Ministry of Education, China Agricultural University, Beijing, China

ARTICLE INFO

Keywords:
Impedance biosensor
Rotary magnetic separation
Cascade reaction
Organic-inorganic hybrid nanoflower
Bacteria detection

ABSTRACT

An impedance biosensor using rotary magnetic separation and cascade reaction was developed for rapid and ultrasensitive detection of *Salmonella typhimurium*. First, magnetic nanoparticles (MNPs) modified with anti-*Salmonella* monoclonal antibodies were injected into a capillary at the presence of a rotary high gradient magnetic field, which was rotated by a stepper motor. Then, a bacterial sample was injected into the capillary and the target bacteria were continuous-flow captured onto the MNPs. After organic-inorganic hybrid nanoflowers were prepared using manganese dioxide (MnO_2), glucose oxidase (GOx) and anti-*Salmonella* polyclonal antibodies (pAbs), they were injected to label the bacteria, resulting in the formation of MNP-bacteria-nanoflower sandwich complexes. Finally, glucose (low conductivity) was injected and oxidized by GOx on the complexes to produce H_2O_2 (low conductivity) and gluconic acid (high conductivity), leading to impedance decrease. Besides, the produced H_2O_2 triggered a cascade reduction of MnO_2 into Mn^{2+}, leading to further impedance decrease. The impedance changes were measured using an interdigitated microelectrode and used to determine the concentration of target bacteria. This biosensor was able to detect *Salmonella* ranging from 10^1 to 10^6 CFU/mL in 2 h with a low detection limit of 10^1 CFU/mL and a mean recovery of 100.1% for the spiked chicken samples.

1. Introduction

Microbiological food poisoning is an important issue globally, which has caused numerous illnesses and huge economic losses (Minor et al., 2015; Oliver et al., 2015). *Salmonella* is one of the most prevalent pathogens (Biggers et al., 2014), and can produce such symptoms as diarrhea, vomiting, gastroenteritis, and severe dehydrating, etc. (Wallis and Galyov, 2010; Bula-Rudas et al., 2015). The existing methods for bacteria detection mainly include traditional culture plating (Cheng et al., 2017), polymerase chain reaction (PCR) (Wei et al., 2018), and enzyme-linked immunosorbent assay (ELISA) (Zhu et al., 2016). However, they require either long time, or complex operations, or specialized instruments, or skilled technicians. Therefore, new methods are needed for rapid and sensitive detection for foodborne pathogens to ensure food safety.

In the past decade, different biosensors have been developed to detect foodborne pathogens, such as quartz crystal microbalance biosensors (Wang et al., 2017a; Yu et al., 2018; Gopalan et al., 2019), surface plasmon resonance biosensors (Nguyen et al., 2016; Chen et al., 2017a), optical biosensors (Tenenbaum and Segal, 2015; Zheng et al., 2019) and electrochemical biosensors (Adkins et al., 2017; Wang et al., 2015a), etc. As a typical electrochemical method, impedance biosensor has been often reported for bacteria detection due to its compact size, simple operation, low cost, easy integration, and high sensitivity (Bernabini et al., 2011; Chen et al., 2015). Recently, some enzymes are frequently used to amplify impedance signals for improving the sensitivity. Among them, glucose oxidase (GOx) (Fu et al., 2013; Xu et al., 2016) and urease (Chen et al., 2015; Wang et al., 2017b; Yao et al., 2018) have received most attentions, because GOx can catalyze the reaction of glucose (low conductivity) into gluconic acid (high conductivity) and hydrogen peroxide (H_2O_2, low conductivity) and urease can catalyze the reaction of urea (low conductivity) into ammonium carbonate (high conductivity). However, their impedance changes result from only one kind of signal molecule and it is not efficient to significantly amplify the impedance signal. Since manganese dioxide (MnO_2) can be reduced to Mn^{2+} in the presence of H_2O_2 (Yuan et al., 2015; Chen

* Corresponding author.
E-mail address: jianhan@cau.edu.cn (J. Lin).

https://doi.org/10.1016/j.bios.2020.112921
Received 25 November 2020; Accepted 18 December 2020
Available online 28 December 2020

et al., 2017b; Lee et al., 2019a; Liu et al., 2018), thus impedance changes might be further enhanced using cascade amplification of impedance signal: the oxidation of glucose by GOx into gluconic acid and H_2O_2, and the cascade reduction of MnO_2 by H_2O_2 into Mn^{2+}.

Specific separation and efficient enrichment of target bacteria from complex background are also crucial for sensitive detection of bacteria in food samples. The conventional immunomagnetic separation is often performed in a centrifuge tube using immune magnetic nanoparticles (MNPs) and a static magnetic field and can separate up to 90% of target bacteria in 1 h, however it could not handle a large volume of sample due to quick attenuation of magnetic field in space. Many efforts have been made on continuous-flow separation of target bacteria from large volumes using MNP chains. Recently, Lee et al. reported an interesting MNP net in a microfluidic channel based on Lenz's law for continuous-flow separation of target bacteria, which was combined with an ATP luminometer and could detect *E. coli* O157:H7 as low as 10^2 CFU/mL in 15 min (Lee et al., 2019b). However, a large amount of immune MNPs were required to ensure high capture efficiency of target bacteria. Since the rotation of MNP clusters, nets or chains could enhance the contact between target bacteria and immune MNPs, immunomagnetic separation might be further improved by rotating MNPs in a fluidic channel.

Based on our previous studies on static magnetic separation using double-layer capillaries for bacteria isolation and concentration (Wang et al., 2017b; Xue et al., 2018; Zhang et al., 2018a) and impedance biosensors using interdigitated microelectrodes for impedance measurement and urease catalysis for signal amplification (Chen et al., 2015; Wang et al., 2017b; Yao et al., 2018), a novel impedance biosensor was proposed for rapid and sensitive detection of *Salmonella* using rotary magnetic separation and impedance signal cascade amplification. As shown in Scheme 1, the biomineralization between bull serum albumin (BSA) and manganese acetate ($MnAC_2$) was first used to prepare the BSA@MnO_2 nanoparticles (BSA@MnO_2 NPs), which were then mixed with GOx, anti-*Salmonella* polyclonal antibodies (pAbs) and calcium chloride ($CaCl_2$) in phosphate buffered saline (PBS) solution to synthesize the immune MnO_2@GOx nanoflowers (MnO_2@GOx NFs). After the MNPs modified with anti-*Salmonella* monoclonal antibodies (mAbs) were injected into the double-layer capillary and formed into rotary MNP chains by rotating the high gradient magnetic field, the bacterial sample and the prepared MnO_2@GOx NFs were successively injected into the capillary to form the MNP-bacteria-MnO_2@GOx complexes. Finally, glucose was injected and oxidized by GOx to produce H_2O_2 and gluconic acid, resulting in the first impedance decrease, and the produced H_2O_2 kept reducing MnO_2 NFs into Mn^{2+}, resulting in the second impedance decrease. The superimposed impedance decrease was measured using the microelectrode and used for quantitative determination of target bacteria.

2. Materials and methods

The materials, the preparation of the bacterial cultures and the synthesis of the immune MNPs could be found in the supplementary material.

2.1. Preparation of the MnO_2@GOx nanoflowers

The MnO_2@GOx nanoflowers were prepared based on the one-step co-precipitation method (Ge et al., 2012) with some modifications. First, the BSA@MnO_2 NPs were prepared according to the biomineralization method (Liu et al., 2012) by mixing 50 μL of 100 mM $MnAC_2$ with 10 mL of BSA (2.5 mg/mL) for 2 min, followed by adding 50 μL of 1

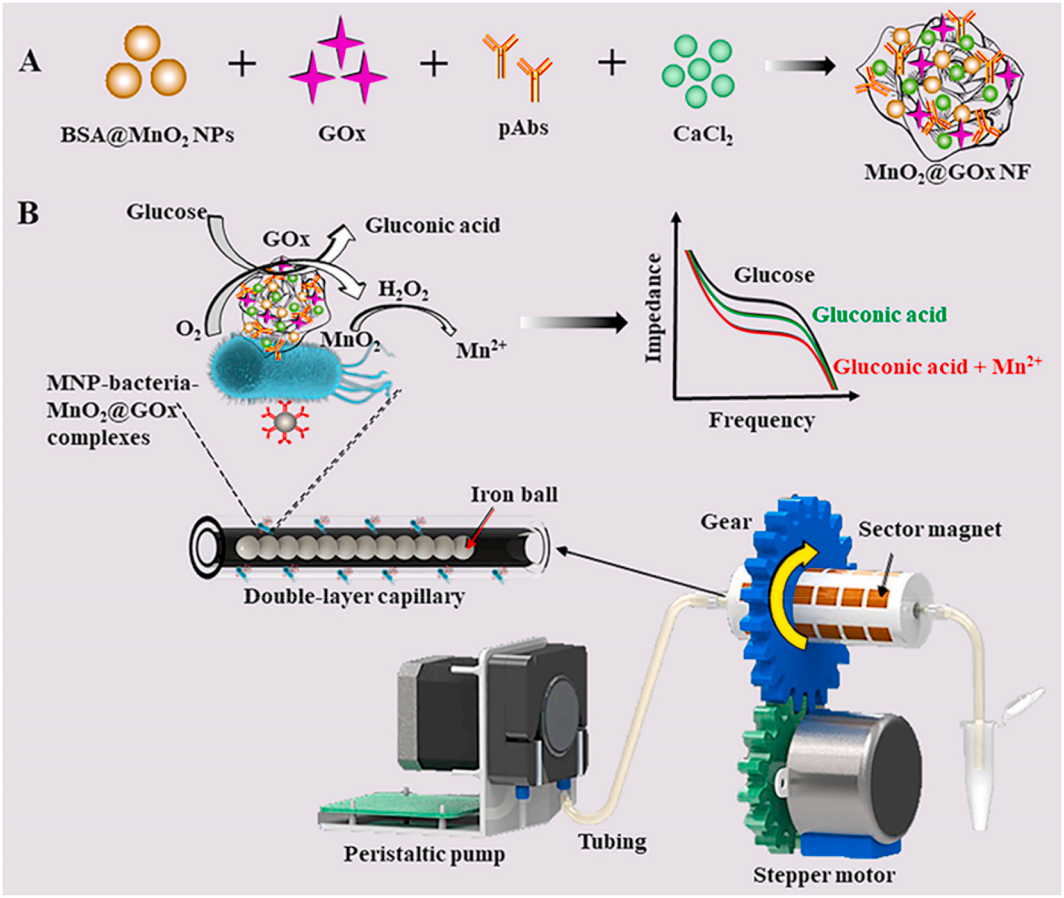

Scheme 1. Schematic of this impedance biosensor for *Salmonella* detection.

M NaOH and stirring for 7 h. Then, the BSA@MnO_2 NPs were obtained by dialyzing with deionized water for 2 d and centrifuging at 15,000 rpm for 30 min three times. Finally, the prepared BSA@MnO_2 NPs, 0.02 mg of the pAbs and 0.18 mg of the GOx were mixed in 1 mL of PBS (3 mM, pH 6.8) containing 20 μL of 200 mM $CaCl_2$ and incubated for 12 h, followed by centrifuging at 12,000 rpm for 10 min and washing with deionized water three times.

2.2. Fabrication of the rotary magnetic separator

The rotary magnetic separator was shown in Fig. S1, mainly including a rotary high gradient magnetic field generator, immune MNPs, and a previously reported double-layer capillary (Wang et al., 2017b; Xue et al., 2018; Zhang et al., 2018a). The rotary magnetic field was generated using a stepper motor to drive two meshing gears and thus rotate 36 sector magnets (internal diameter: 5 mm; external diameter: 15 mm; thickness: 5 mm; angle: 30^0; grade: N52; material: NdFeB) at the speed of 3 rpm. The magnets were mounted with the mutually repelling layout in a 3D printed holder. A cylindrical hole in the center of the holder was used to concentrically house the double-layer capillary with the diameter of 3.0 mm and the length of 60 mm, allowing the rotary magnetic field to magnetize the iron balls in the capillary and thus generate local high gradient magnetic fields. More details about the sector magnets and the holder could be found in Fig. S2. The capillary was connected to a peristaltic pump using the tubing and hoses for injection of the MNPs, the bacterial sample and the MnO_2@GOx NFs.

2.3. Separation of the target bacteria

Prior to bacterial separation, the capillary, the tubing and centrifuge tube were cleaned with 75% alcohol for 45 min and rinsed with deionized water, followed by blocking with 1% BSA for 30 min to minimize the non-specific adsorption and rinsing with deionized water. First, 40 μg of the immune MNPs were injected into the capillary at the presence of the rotary magnetic field and recycled three times to ensure stable capture of most MNPs and uniform distribution in the capillary. Then, 1 mL of the bacterial sample at each concentration from 10^1 to 10^6 CFU/mL was injected into the capillary at the flow rate of 0.15 mL/min and recycled for 20 min. Finally, the capillary was washed with PBS to remove the residual background.

2.4. Detection of the target bacteria

After the target bacteria were captured by the immune MNPs in the capillary, the MnO_2@GOx NFs were first injected into the capillary at the flow rate of 0.15 mL/min and recycled for 40 min to form the MNP-bacteria-MnO_2@GOx sandwich complexes, followed by continuous-flow washing with deionized water to remove the unbound MnO_2@GOx NFs and residual ions. Then, 200 μL of 10 mM glucose was injected into the capillary and recycled for 30 min, allowing the oxidation of glucose into gluconic acid and H_2O_2 and the cascade reduction of MnO_2 into Mn^{2+}. Finally, the electrochemical impedance spectra (EIS) were measured using the electrochemical workstation (IM6, Zahner, Kronach, Bavaria, Germany) to apply a sinusoidal wave with the frequency of 1 Hz-1 MHz and the magnitude of 5 mV on the interdigitated microelectrode with the finger width and space of 15 μm, and the impedance change at the characteristic frequency of 10 kHz was calculated for determination of the target bacteria.

3. Results and discussion

3.1. Concept proof of this impedance biosensor

The rotary magnetic separation of the target bacteria plays an important role in this impedance biosensor. The COSMOL software was used to simulate the magnetic field. As shown in Fig. S3, the iron balls in the double-layer capillary are magnetized by the repelling sector magnets to generate local high gradient magnetic fields in the ring channel. Besides, it is found from the COMSOL simulation that this magnetic field has a mean gradient of ~200 T/m, which is around 10 times higher than many commercial magnetic separators. Therefore, when the MNPs were injected into the capillary, they were captured by these high gradient magnetic fields against the walls of the ring channel and slowly rotated with the rotatory sector magnets.

This impedance biosensor was based on the impedance change due to two cascade reaction: (1) glucose with low conductivity was oxidized by the GOx to produce H_2O_2 with low conductivity and gluconic acid with high conductivity (see equation (1)), resulting in the increase on iron strength and thus the decrease on impedance; (2) MnO_2 was reduced by the produced H_2O_2 into Mn^{2+} (see equation (2)), resulting in the further increase on iron strength and thus the further decrease on impedance. Thus, it is essential to verify the low impedance (high conductivity) of gluconic acid and the high impedance (low conductivity) of glucose, H_2O_2 and MnO_2.

$$Glucose + O_2 \rightarrow Gluconic\ acid\ + H_2O_2 \quad (1)$$

$$MnO_2 + H_2O_2 \rightarrow Mn^{2+} + H_2O \quad (2)$$

Therefore, electrochemical impedance spectra (EIS) for different concentrations of gluconic acid, glucose, H_2O_2 and the mixture of H_2O_2 and MnO_2 were measured using the microelectrode on the electrochemical station. As shown in Fig. 1a and b, when the concentration of either glucose or H_2O_2 increases from 1 μM to 10 mM, their impedance at the characteristic frequency of 10 kHz almost remains at the same level (~60.0 kΩ), verifying that both glucose and H_2O_2 have a low ion strength (low conductivity), i.e., they do not change with their concentration. As shown in Fig. 1c, the impedance at 10 kHz decreases with the increase of the concentration of gluconic acid, and a good linear relationship between the impedance change (ΔZ) and the concentration (C) from 100 nM to 100 μM is found and can be described as $\Delta Z = 6.18*\ln C + 17.26$ ($R^2 = 0.99$) (Fig. 1d), verifying that gluconic acid has an obviously higher conductivity than glucose and H_2O_2, and can be determined by measuring its impedance.

To verify the feasibility of impedance change due to H_2O_2 reduction of MnO_2, excessive amount (1 mg) of MnO_2 nanoparticles were mixed with each concentration of H_2O_2 from 100 nM to 100 μM for 10 min. After the remained MnO_2 nanoparticles were discarded by centrifugation at 10, 000 rpm, the impedance of the mixture was measured and shown in Fig. 1e. When the concentration of H_2O_2 increases from 100 nM to 100 μM, the impedance decreases from 54.0 kΩ to 7.9 kΩ, indicating that MnO_2 nanoparticles are reduced into Mn^{2+} and thus this results in the increase on iron strength and the decrease on impedance. Besides, a good linear relationship between the impedance change at the characteristic frequency of 10 kHz and the concentration of H_2O_2 is found and can be expressed as $\Delta Z = 6.63*\ln C + 22.22$ ($R^2 = 0.99$) (Fig. 1f).

To further demonstrate the effect of cascade reaction on the impedance change, the same amount (50 μg) of GOx was used to oxidize each concentration (1 μM, 10 μM and 50 μM) of glucose with the excessive amount of MnO_2 nanoparticles, and the impedance was measured and compared with that for the same amount of GOx to oxidize the same concentration of glucose without MnO_2 nanoparticles. The impedance change rate ($\Delta Z\%$) was used to evaluate the effect of cascade reaction on the impedance change and defined as:

$$\Delta Z\% = \frac{\Delta Z_2 - \Delta Z_1}{\Delta Z_1} \quad (3)$$

where, ΔZ_1 and ΔZ_2 are the impedance changes due to GOx oxidation of glucose without and with MnO_2, respectively. As shown in Fig. 1g, the impedance change rate increases from 22.5% to 32.5%, when the

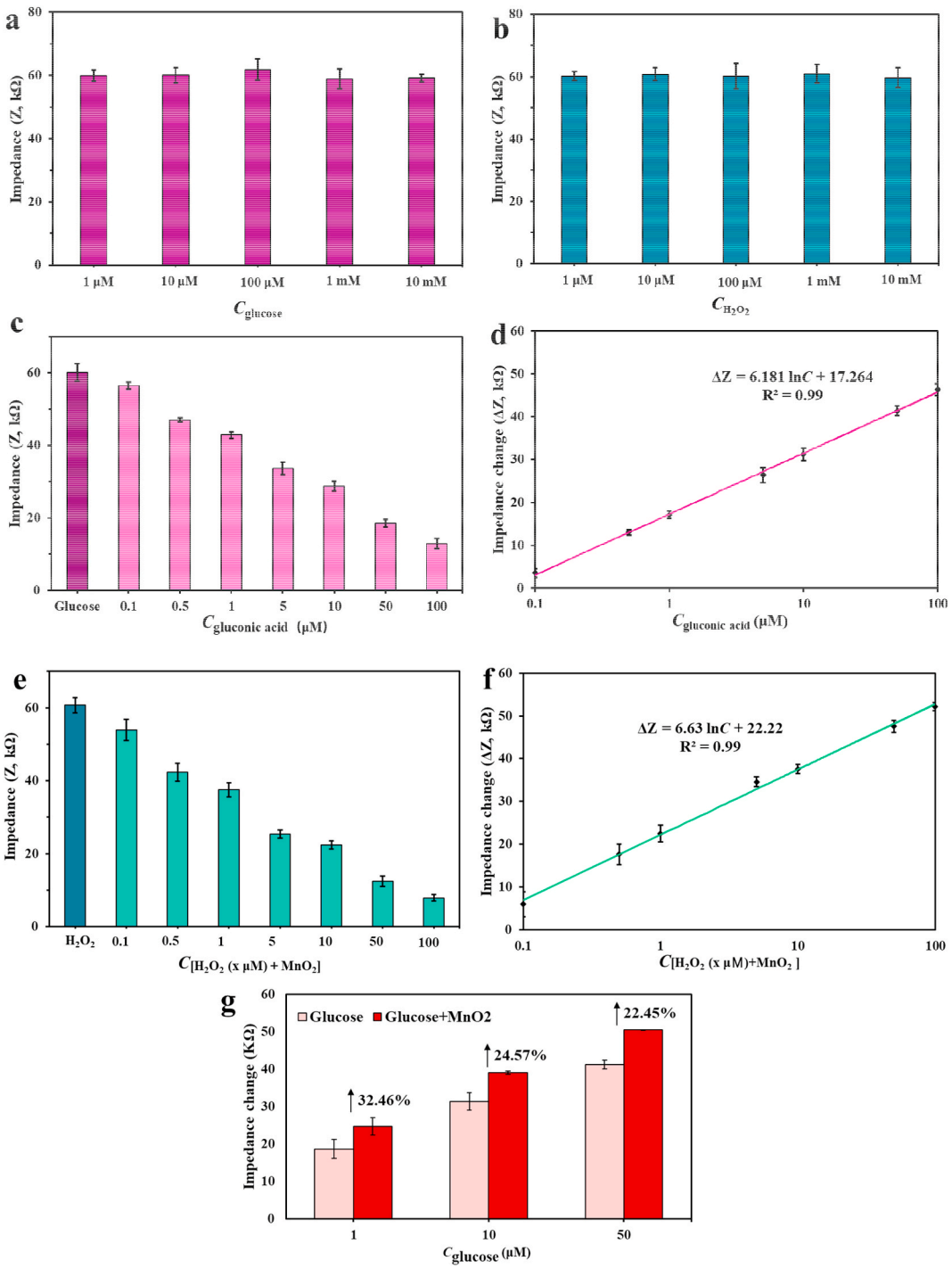

Fig. 1. Concept proof of this impedance biosensor. (a) The impedance for different concentrations (1 μM–10 mM) of glucose. (b) The impedance for different concentrations (1 μM–10 mM) of H_2O_2. (c) The impedance for different concentrations (0.1–100 μM) of gluconic acid. (d)The linear relationship between the impedance change and the concentration of gluconic acid. (e) The impedance for the mixture of excessive amount (1 mg) of MnO_2 nanoparticles and different concentrations (0.1–100 μM) of H_2O_2. (f) The linear relationship between the impedance change and the concentration of H_2O_2. (g) The impedance changes for different concentrations (1–50 μM) of glucose oxidized by the GOx with and without MnO_2 nanoparticles.

concentration of glucose changes from 1 to 50 μM, indicating that the cascade reaction is effective to enhance the amplification of impedance signal.

3.2. Characterization of the BSA@MnO_2 NPs and MnO_2@GOx NFs

The successful synthesis of the BSA@MnO_2 NPs and MnO_2@GOx NFs is crucial to the development of this impedance biosensor. Due to its strong affinity towards inorganic salts, the most abundant plasma protein, BSA, was used for biomineralization to prepare the BSA@MnO_2 NPs, which were characterized using transmission electron microscopy (TEM). As shown in Fig. 2a, the BSA@MnO_2 NPs are homogeneous and monodispersed with the average size of ~4 nm, indicating successful synthesis of the BSA@MnO_2 NPs through the biomineralization between BSA and $MnAC_2$. Besides, the prepared BSA@MnO_2 NPs were used to further react with GOx, pAbs and $CaCl_2$ through the coordination of

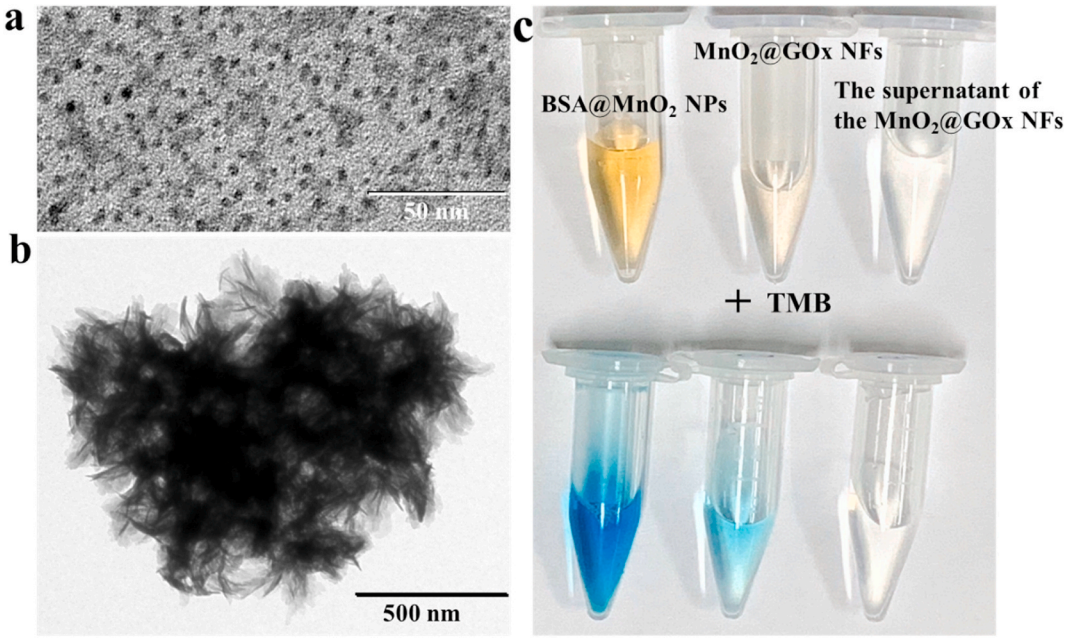

Fig. 2. Characterization of the BSA@MnO_2 NPs and MnO_2@GOx NFs. (a) The TEM image of the BSA@MnO_2 NPs. (b) The TEM image of the MnO_2@GOx NFs. (c) The color change after the BSA@MnO_2 NPs and the MnO_2@GOx NFs were mixed with TMB.

amide groups on the protein backbone between the inorganic ions (calcium ions and hydrophosphate ions) and the proteins (BSA, GOx and pAb) to prepare the MnO_2@GOx NFs, which were also characterized using TEM. As shown in Fig. 2b, the MnO_2@GOx NFs are monodispersed with the average size of ~1.2 μm and have an obvious flower morphology, indicating successful synthesis of the MnO_2@GOx NFs.

To further verify successful loading of the MnO_2 NPs in the MnO_2@GOx NFs, both the BSA@MnO_2 NPs and the MnO_2@GOx NFs were mixed with 3,3′,5,5′-tetramethylbenzidine (TMB) to observe the color change, respectively, as MnO_2 was previously reported to exhibit peroxidase- and oxidase-like activities (Liu et al., 2012, 2013). As shown in Fig. 2c, the dark brown BSA@MnO_2 NPs turn into dark blue after mixing with TMB, indicating successful preparation of BSA@MnO_2 NPs. The light brown MnO_2@GOx NFs also change into light blue after mixing with TMB, indicating successful loading of MnO_2 NPs in the MnO_2@GOx NFs. Besides, the colorless supernatant during the

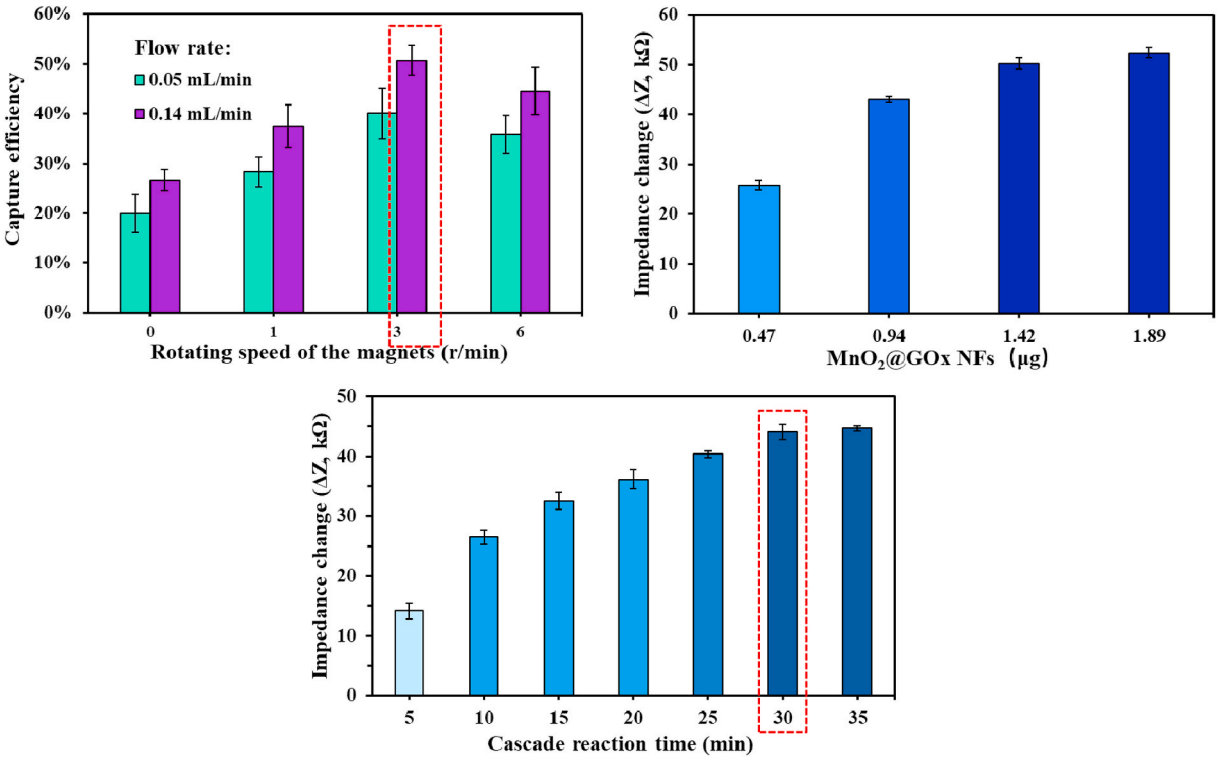

Fig. 3. Optimization of this impedance biosensor. (a) The rotating speed of the magnetic field. (b) The amount of the MnO_2@GOx NFs. (c) The time for the cascade reaction.

preparation of the MnO_2@GOx NFs does not have visible color change after mixing with TMB, indicating that almost all the BSA@ MnO_2 NPs have participated in the forming of the MnO_2@GOx NFs.

3.3. Optimization of this impedance biosensor

The flow rate for injecting the sample and the speed for rotating the magnetic fields have an important impact on continuous-flow separation of the target bacteria. Thus, two flow rates (0.05 and 0.15 mL/min) and three rotating speeds (0, 1, 3 and 6 rpm) were compared to separate the target bacteria. As shown in Fig. 3a, when the rotating speed changes from 0 to 6 rpm, the separation efficiency first increases and then decreases with a maximum of ~50% at 3 rpm. This was because the rotation of the MNPs at low speed (from 0 to 3 rpm) increased the contact between the MNPs and the bacteria, allowing the capture of more target bacteria. However, when the speed kept increasing from 3 to 6 rpm, more bacteria were not captured due to insufficient immunoreaction although the contact between the MNPs and the bacteria was still enhanced. Besides, when the separation time is fixed at 20 min, the separation efficiency for the flow rate of 0.15 mL/min is higher than that for 0.05 mL/min. This was mainly because the bacterial sample were cycled three times for 0.15 mL/min, however only one time for 0.05 mL/min. Thus, the optimal rotating speed of 3 rpm and the optimal flow rate of 0.15 mL/min were used.

The amount of the MnO_2@GOx NFs is also optimized. Different amounts of the MnO_2@GOx NFs from 0.47 to 1.89 μg (BSA content) were compared for detection of the target bacteria. As shown in Fig. 3b, when the amount of the MnO_2@GOx NFs changes from 0.47 μg to 1.42 μg, the impedance change increases from 25.6 to 50.3 kΩ. The further increase on the amount of MnO_2@GOx NFs to 1.89 μg only results in 4.3% increase on the impedance change. Thus, the optimal amount of 1.42 μg for the MnO_2@GOx NFs was used.

Besides, the cascade reaction time for the GOx to oxidize glucose and for H_2O_2 to reduce MnO_2 is crucial to this biosensor. Different cascade reaction time from 5 to 35 min was compared. As shown in Fig. 3c, when the time changes from 5 to 30 min, the impedance change increases from 14.2 to 44.1 kΩ because more gluconic acid and Mn^{2+} are produced, resulting in lower impedance. The further increase on the time to 35 min only leads to 1.4% increase on the impedance change. Thus, the optimal time of 30 min for the cascade reaction time was used.

3.4. Calibration model of this impedance biosensor

To establish the calibration model for this biosensor, different concentrations of the target bacteria from 1×10^1 to 1×10^6 CFU/mL were detected under the optimal conditions. The electrochemical impedance spectra were shown in Fig. 4a. The impedance decreases with the increase of bacterial concentration from 1×10^1 to 1×10^6 CFU/mL, because more MNP-bacteria-MnO_2@GOx sandwich complexes are formed, resulting in more gluconic acid and Mn^{2+}. The impedance at the characteristic frequency of 10 kHz for different concentrations was plotted to obtain the calibration curve. As shown in Fig. 4b, a good linear relationship between the impedance change (ΔZ) and the bacterial concentration from 1×10^1 to 1×10^6 CFU/mL is found and can be expressed as $\Delta Z = 3.11 * \ln C + 5.42$ ($R^2 = 0.98$). Based on three times of signal to noise ratio, the limit of detection (LOD) of this biosensor was calculated as 1×10^1 CFU/mL. Compared to some recently reported methods in Table 1, including electrochemical, optical, ELISA and real-time PCR, this biosensor has shown a higher sensitivity and/or a shorter detection time. This is because (1) the use of the rotary magnetic field for specific separation and efficient concentration of the target bacteria in a short time (50% separation efficiency in 20 min); (2) the application of the cascade reaction for effective amplification of the impedance signal (26.3% more than non-cascade reaction); (3) the employment of the microelectrode for sensitive measurement of the impedance change (linear range: 1–100 μM). Besides, the TEM imaging was conducted to verify the successful formation of the MNP-bacteria-MnO_2@GOx sandwich complexes. As shown in Fig. 4c, the sandwich complexes were

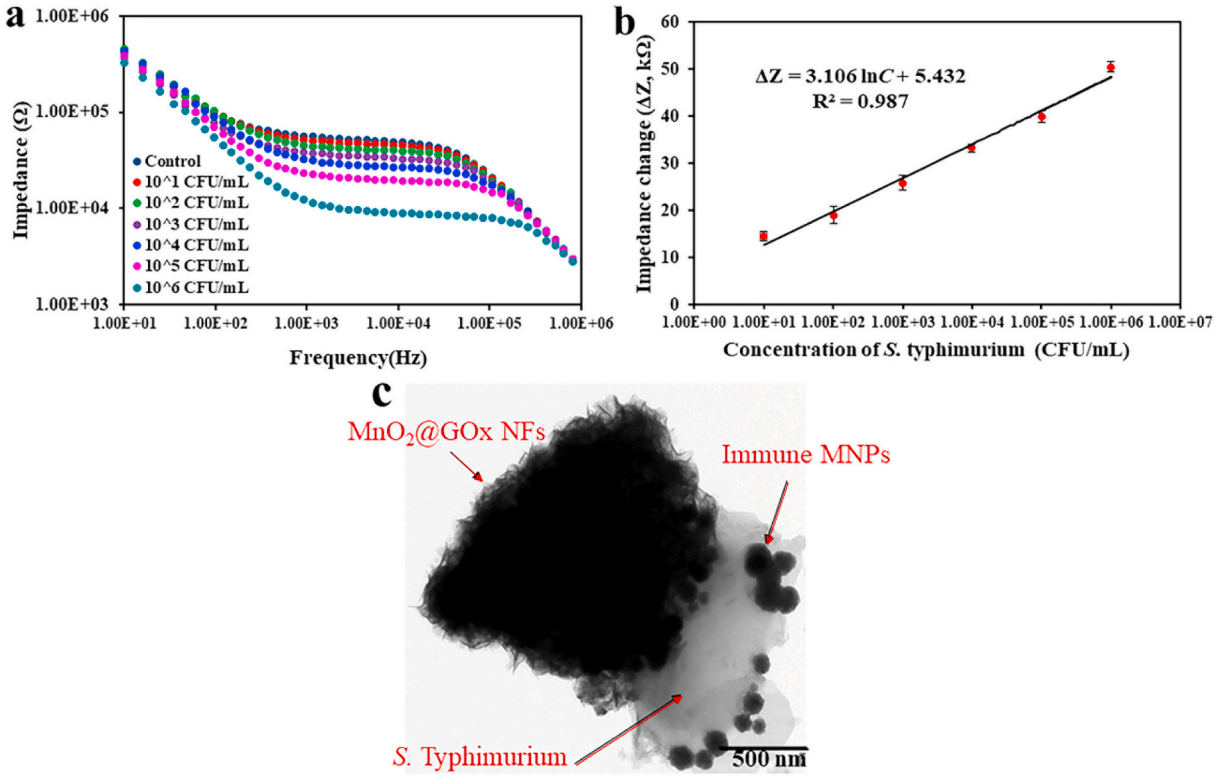

Fig. 4. (a) The electrochemical impedance spectra for different concentrations of *Salmonella typhimurium* from 1×10^1 to 1×10^6 CFU/mL. (b) The calibration model of this biosensor. (c) The TEM image of the MNP-bacteria-MnO_2@GOx sandwich complexes.

Table 1
Comparison of this biosensor with some reported methods for foodborne pathogen detection.

Methods	Linear Range (CFU/mL)	LOD (CFU/mL)	Ref
Electrochemical	1.0×10^3 to 1.0×10^8	1.0×10^3	Farka et al. (2016)
Colorimetric	1.0×10^2 to 1.0×10^7	1.0×10^2	Srisa-Art et al. (2018)
Fluorescent	2.5×10^3 to 1.95×10^8	5.0×10^2	Kuang et al. (2013)
Raman Spectroscopy	1.0×10^1 to 1.0×10^7	6.6×10^1	Draz and Lu (2016)
Quartz Crystal Microbalance	1.0×10^2 to 1.0×10^6	1.0×10^2	Ozalp et al. (2015)
Surface Plasmon Resonance	1.0×10^3 to 1.0×10^7	7.4×10^3	Vaisocherová-Lísalová et al. (2016)
ELISA	1.0×10^4 to 2.8×10^6	9.0×10^2	Zhu et al. (2016)
Real-time PCR	2.5×10^3 to 2.5×10^6	1.2×10^2	Zhang et al. (2018b)
Isothermal PCR	1.7×10^2 to 1.7×10^4	1.7×10^2	Trinh and Lee (2018)
This study	1.0×10^1 to 1.0×10^6	1.0×10^1	–

clearly observed, including the MNPs (~150 nm), the target bacteria (~1.2 μm) and the MnO_2@GOx NFs (~1.2 μm).

3.5. Specificity and applicability of this biosensor

The specificity of this impedance biosensor was investigated using *E. coli* O157:H7, *Listeria monocytogenes*, *Staphylococcus aureus* and *Bacillus cereus* as non-target bacteria. Besides, the target bacteria, non-target bacteria and the mixture of all the bacteria at the concentration of 1×10^6 CFU/mL were detected using this biosensor. The procedures for the non-target bacteria and mixture detection were the same as that for the target bacteria. As shown in Fig. 5a, the impedance change for the target bacteria (50.4 kΩ) is much larger than those for each non-target bacteria at the same concentration and the negative control, and has a comparable level with that for the mixture, indicating that this biosensor has a good specificity due to the use of specific antibodies against the target bacteria.

To further evaluate the feasibility of this biosensor for practical application, chicken meats were purchased from a local supermarket and verified to be free of the target bacteria using the conventional selective culture plating (Zhang et al., 2019). The spiked chicken meat samples were prepared by mixing 25 g of chicken meat with 225 mL of sterile PBS and homogenizing the mixture for 3 min. After standing for

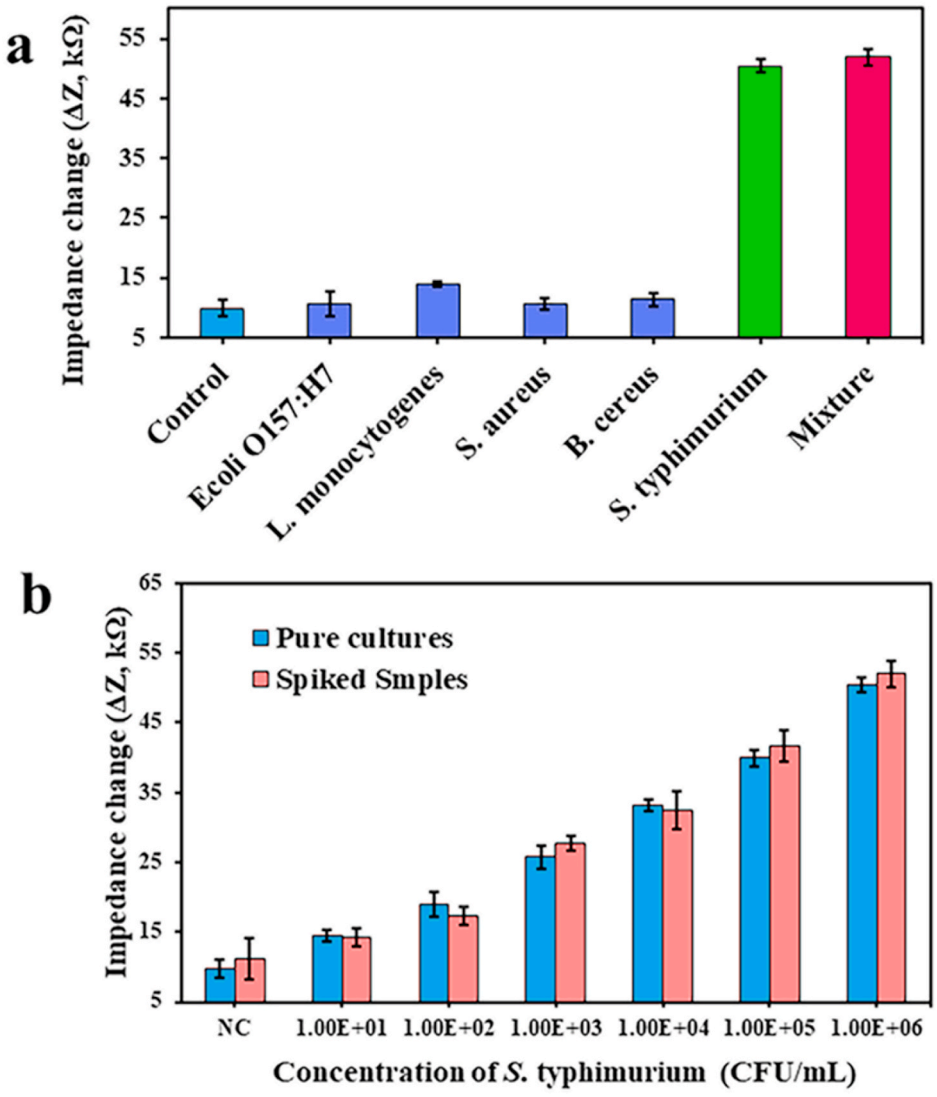

Fig. 5. (a) The specificity of this biosensor. (b) The applicability of this biosensor for detection of *Salmonella* in spiked chicken meats.

10 min to obtain the supernatant, different concentrations of target bacteria were added to obtain the spiked samples, which were finally detected using this biosensor. As shown in Fig. 5b, the impedance changes for the spiked chicken samples are slightly different from those for the pure bacterial cultures at the same concentration, respectively. The differences are mainly due to the interferences from the proteins, fat and other molecules in the chicken meats (Wang et al., 2015b). The recovery was defined as the ratio of the detected concentration to the added one and calculated as 97.4%, 88.2%, 109.4%, 97.2%, 105.1% and 103.5% for different concentrations from 10^1 to 10^6 CFU/mL. The mean recovery was 100.1%, verifying the applicability of this biosensor for detection of target bacteria in real samples.

4. Conclusions

An impedance biosensor was successfully developed for rapid and sensitive detection of *Salmonella* using the rotary magnetic separation in the double-layer capillary for continuous-flow separation of target bacteria and the cascade reaction for effective amplification of the impedance signal. The separation efficiency of *Salmonella* using this rotary magnetic separation method was ~50% within only 20 min. The cascade reaction was demonstrated to improve the impedance change up to 32.5%. This biosensor was able to quantitatively detect *Salmonella typhimurium* from 10^1 to 10^6 CFU/mL in 2 h with the detection limit of 10^1 CFU/mL. The biosensor can be further improved by separating the target bacteria from larger volume, enhancing the stability of the MnO_2@GOx NFs, and increasing the circulation of the bacterial sample.

Declaration of competing interest

The authors declare that they have no known competing financial interests or personal relationships that could have appeared to influence the work reported in this paper.

Acknowledgments

This study was supported in part by the National Natural Science Foundation of China (32071899), the Walmart Foundation (SA1703161) and the Walmart Food Safety Collaboration Center.

Appendix A. Supplementary data

Supplementary data to this article can be found online at https://doi.org/10.1016/j.bios.2020.112921.

References

Adkins, J.A., Boehle, K., Friend, C., Chamberlain, B., Bisha, B., Henry, C.S., 2017. Colorimetric and electrochemical bacteria detection using printed paper- and transparency-based analytic devices. Anal. Chem. 89, 3613–3621.
Bernabini, C., Holmes, D., Morgan, H., 2011. Micro-impedance cytometry for detection and analysis of micron-sized particles and bacteria. Lab Chip 11, 407–412.
Biggers, H.M., Lester, R., Nadjm, B., Crump, J.A., 2014. Invasive *Salmonella* infections in areas of high and low malaria transmission intensity in Tanzania. Clin. Infect. Dis. 58, 638–647.
Bula-Rudas, F.J., Rathore, M.H., Maraqa, N.F., 2015. Salmonella infections in childhood. Adv. Pediatr. 62, 29–58.
Chen, Q., Lin, J., Gan, C., Wang, Y., Wang, D., Xiong, Y., Lai, W., Li, Y., Wang, M., 2015. A sensitive impedance biosensor based on immunomagnetic separation and urease catalysis for rapid detection of *Listeria monocytogenes* using an immobilization-free interdigitated array microelectrode. Biosens. Bioelectron. 74, 504–511.
Chen, J., Park, B., Eady, M., 2017a. Simultaneous Detection and serotyping of *Salmonellae* by immunomagnetic separation and label-free surface-enhanced Raman spectroscopy. Food. Anal. Method. 10, 3181–3193.
Chen, J.-L., Li, L., Wang, S., Sun, X.-Y., Xiao, L., Ren, J.-S., et al., 2017b. A glucose-activatable trimodal glucometer self-assembled from glucose oxidase and MnO_2 nanosheets for diabetes monitoring. J. Mater. Chem-B 5, 5336–5344.
Cheng, N., Song, Y., Zeinhom, M.M.A., Chang, Y.C., Sheng, L., Li, H., et al., 2017. Nanozyme-mediated dual immunoassay integrated with smartphone for use in simultaneous detection of pathogens. ACS Appl. Mater. Interfaces 9, 40671–44080.
Draz, M.S., Lu, X., 2016. Development of a loop mediated isothermal amplification (LAMP) - surface enhanced Raman spectroscopy (SERS) assay for the detection of *Salmonella* Enterica serotype enteritidis. Theranostics 6, 522–532.
Farka, Z., Juřík, T., Pastucha, M., Kovář, D., Lacina, K., Skládal, P., 2016. Rapid immunosensing of *Salmonella* Typhimurium using electrochemical impedance spectroscopy: the effect of sample treatment. Electroanalysis 28, 1803–1809.
Fu, Y., Callaway, Z., Lum, J., Wang, R., Lin, J., Li, Y., 2013. Exploiting enzyme catalysis in ultra-low ion strength media for impedance biosensing of avian influenza virus using a bare interdigitated electrode. Anal. Chem. 86, 1965–1971.
Ge, J., Lei, J., Zare, R.N., 2012. Protein-inorganic hybrid nanoflowers. Nat. Nanotechnol. 7, 428–432.
Gopalan, S.A., Arumugam, S., Mercy, R.B., Gurwinder, S., Ajayan, V., 2019. Recent progress on the sensing of pathogenic bacteria using advanced nanostructures. Bull. Chem. Soc. Jpn. 92, 216–244.
Kuang, H., Cui, G., Chen, X., Yin, H., Yong, Q., Xu, L., et al., 2013. A one-step homogeneous sandwich immunosensor for *Salmonella* detection based on magnetic nanoparticles (MNPs) and auantum dots (QDs). Int. J. Mol. Sci. 14, 8603–8610.
Lee, P.C., Li, N.S., Hsu, Y.P., Peng, C., Yang, H.W., 2019a. Direct glucose detection in whole blood by colorimetric assay based on glucose oxidase-conjugated graphene oxide/MnO_2 nanozymes. Analyst 144, 3038–30344.
Lee, H., Kim, G., Park, E., Jeon, S., 2019b. Lenz's law-based virtual net for detection of pathogenic bacteria from water. Anal. Chem. 91, 15585–15590.
Liu, X., Wang, Q., Zhao, H., Zhang, L., Su, Y., Lv, Y., 2012. BSA-templated MnO_2 nanoparticles as both peroxidase and oxidase mimics. Analyst 137, 4552–4558.
Liu, X., Wang, Q., Zhao, H., Zhang, L., Su, Y., Lv, Y., 2013. Colorimetric detection of glutathione in human blood serum based on the reduction of oxidized TMB. New J. Chem. 37, 2174–2178.
Liu, Z., Xianyu, Y., Zheng, W., Zhang, J., Luo, Y., Chen, Y., et al., 2018. T_1-mediated nanosensor for immunoassay based on an activatable MnO_2 nanoassembly. Anal. Chem. 90, 2765–2771.
Minor, T., Lasher, A., Klontz, K., Brown, B., Nardinelli, C., Zorn, D., 2015. The per case and total annual costs of foodborne illness in the United States, Risk. Anal 35, 1125–1139.
Nguyen, H.H., Yi, S.Y., Woubit, A., Kim, M., 2016. A portable surface plasmon resonance biosensor for rapid detection of *Salmonella* typhimurium. Appl. Sci. Conver. Technol. 25, 61–65.
Oliver, S.P., Jayarao, B.M., Almeida, R.A., 2015. Foodborne pathogens in milk and the dairy farm environment: food safety and public health implications. Foodb. Pathog. Dis. 2, 115–129.
Ozalp, V.C., Bayramoglu, G., Erdem, Z., Arica, M.Y., 2015. Pathogen detection in complex samples by quartz crystal microbalance sensor coupled to aptamer functionalized core-shell type magnetic separation. Anal. Chim. Acta 853, 533–540.
Srisa-Art, M., Boehle, K.E., Geiss, B.J., Henry, C.S., 2018. Highly sensitive detection of *Salmonella* typhimurium using a colorimetric paper-based analytical device coupled with immunomagnetic separation. Anal. Chem. 90, 1035–1043.
Tenenbaum, E., Segal, E., 2015. Optical biosensors for bacteria detection by a peptidomimetic antimicrobial compound. Analyst 140, 7726–7733.
Trinh, T.N.D., Lee, N.Y., 2018. A rapid and eco-friendly isothermal amplification microdevice for multiplex detection of foodborne pathogens. Lab Chip 18, 2369–2377.
Vaisocherová-Lísalová, H., Víšová, I., Ermini, M.L., Špringer, T., Song, X.C., Mrázek, J., et al., 2016. Low-fouling surface plasmon resonance biosensor for multi-step detection of foodborne bacterial pathogens in complex food samples. Biosens. Bioelectron. 80, 84–90.
Wallis, T.S., Galyov, E.E., 2010. Molecular basis of *Salmonella*-induced enteritis. [J]. Mol. Microbiol. 36, 997–1005.
Wang, Y., Wang, D., Xiong, Y., et al., 2015a. A sensitive impedance biosensor based on immunomagnetic separation and urease catalysis for rapid detection of *Listeria monocytogenes* using an immobilization-free interdigitated array microelectrode. Biosens. Bioelectron. 74, 504–511.
Wang, R., Lum, J., Callaway, Z., Lin, J., Bottje, W., Li, Y., 2015b. A label-free impedance immunosensor using screen-printed interdigitated electrodes and magnetic nanobeads for the detection of *E. coli* O157:H7. Biosensors 5, 791–803.
Wang, L., Wang, R., Chen, F., Jiang, T., Wang, H., Slavik, M., et al., 2017a. QCM-based aptamer selection and detection of *Salmonella* typhimurium. Food Chem. 221, 776–782.
Wang, L., Huang, F., Cai, G., Yao, L., Zhang, H., Lin, J., 2017b. An electrochemical aptasensor using coaxial capillary with magnetic nanoparticle, urease catalysis and PCB electrode for rapid and sensitive detection of *Escherichia coli* O157:H7. Nanotheranostics 1, 403–414.
Wei, C., Zhong, J., Hu, T., Zhao, X., 2018. Simultaneous detection of *Escherichia coli* O157:H7, *Staphylococcus aureus* and *Salmonella* by multiplex PCR in milk. Biotechnology 8, 76.
Xu, M., Wang, R., Li, Y., 2016. Rapid detection of *Escherichiacoli* O157:H7and *Salmonella* Typhimurium in foods using an electrochemical immunosensor based on screen-printed interdigitated microelectrode and immunomagnetic separation. Talanta 148, 200–208.
Xue, L., Zhang, L., Zhang, H., Jin, X., Lin, J., 2018. An ultrasensitive fluorescent biosensor using high gradient magneticseparation and quantum dots for fast detection of foodborne pathogenic bacteria. Sensor. Actuator. B Chem. 265, 318–325.
Yao, L., Wang, L., Huang, F., Cai, G., Xi, X., Lin, J., 2018. A microfluidic impedance biosensor based on immunomagneticseparation and urease catalysis for continuous-flow detection of *E. coli* O157:H7. Sensor. Actuator. B Chem. 259, 1013–1021.
Yu, X., Chen, F., Wang, R., Li, Y., 2018. Whole-bacterium SELEX of DNA aptamers for rapid detection of *E.coli* O157:H7 using a QCM sensor. J. Biotechnol. 266, 39–49.

Yuan, J., Cen, Y., Kong, X.J., Wu, S., Liu, C.L., Yu, R.Q., et al., 2015. MnO_2-nanosheet-modified upconversion nanosystem for sensitive turn-on fluorescence detection of H_2O_2 and glucose in blood. ACS Appl. Mater. Interfaces 7, 10548–10555.
Zhang, H., Huang, F., Cai, G., Li, Y., Lin, J., 2018a. Rapid and sensitive detection of *Escherichia coli* O157:H7 using coaxial channel-based DNA extraction and microfluidic PCR. J. Dairy Sci. 101, 9736–9746.
Zhang, J., Khan, I., Zhang, Q., Liu, X., Dostalek, J., Liedberg, B., et al., 2018b. Lipopolysaccharides detection on a grating-coupled surface plasmon resonance smartphone biosensor. Biosens. Bioelectron. 99, 312–317.
Zhang, H., Xue, L., Huang, F., Wang, S., Wang, L., Liu, N., Lin, J., 2019. A capillary biosensor for rapid detection of *Salmonella* using Fe-nanocluster amplification and smartphone imaging. Biosens. Bioelectron. 127, 142–149.
Zheng, L., Cai, G., Wang, S., Liao, M., Li, Y., Lin, J., 2019. A microfluidic colorimetric biosensor for rapid detection of *Escherichia coli* O157:H7 using gold nanoparticle aggregation and smart phone imaging. Biosens. Bioelectron. 124, 143–149.
Zhu, L., He, J., Cao, X., Huang, K., Luo, Y., Xu, W., 2016. Development of a double-antibody sandwich ELISA for rapid detection of *Bacillus Cereus* in food. Sci. Rep. 6, 16092.